

# Absolute Calibration of ATMS Upper Level Temperature

## Sounding Channels Using GPS RO Observations

Xiaolei Zou<sup>1,2\*</sup>, Lin Lin<sup>3,4</sup>, and Fuzhong Weng<sup>5</sup>

<sup>1</sup>Center of Data Assimilation for Research and Application, Nanjing University of Information and Science & Technology, Nanjing, China

<sup>2</sup>Department of Earth, Ocean and Atmospheric Sciences, Florida State University, USA

<sup>3</sup>Joint Center for Satellite Data Assimilation, College Park, Maryland, USA

<sup>4</sup>Earth Resources Technology, Inc. Laurel, Maryland, USA

<sup>5</sup>National Environmental Satellite, Data, & Information Service, National Oceanic and Atmospheric Administration, Washington, D. C., USA

*IEEE Trans. Geosci. Remote Sens.*

September 2012

---

\*Corresponding author: Dr. X. Zou, Department of Earth, Ocean and Atmospheric Science, Florida State University, Tallahassee, FL 32306-4520, USA. Email: [xzou@fsu.edu](mailto:xzou@fsu.edu). Phone: 850-644-6025.

## **Abstract**

The absolute accuracy of antenna brightness temperatures (TDR) from the Advanced Technology Microwave Sounder (ATMS) onboard the Suomi National Polar-orbiting Partnership (NPP) satellite is estimated using Constellation Observing System for Meteorology, Ionosphere, and Climate (COSMIC) Radio Occultation (RO) data as input to the U.S. Joint Center of Satellite Data Assimilation (JCSDA) Community Radiative Transfer Model (CRTM). It is found that the mean differences (e.g., biases) of observed TDR observations to GPS RO simulations are positive for channels 6, 10-13 with values smaller than 0.5K and negative for channels 5, 7-9 with values greater than -0.7K. The bias distribution is slightly asymmetric across the scan line. A line-by-line radiative transfer model is used to further understand the sources of errors in forward calculations. It is found that for some channels, the bias can be further reduced in a magnitude of 0.3K if the accurate line-by-line simulations are used. With the high quality of GPS RO observations and the accurate radiative transfer model, ATMS upper level temperature sounding channels are calibrated with known absolute accuracy. After the bias removal in ATMS TDR data, it is shown that the distribution of residual errors for ATMS channels 5-13 is close to a normal Gaussian one. Thus, for these channels, the ATMS antenna brightness temperature can be absolutely calibrated to the sensor brightness temperature without a systematic bias.

## 1. Introduction

The Suomi National Polar-orbiting Partnership (SNPP) satellite is the pathfinder in building up the next-generation satellite system that will take over NASA's Earth Observing System (EOS) satellites launched in the last decade. It was successfully launched on October 28, 2011 from Vandenberg Air Force Base, California. The Advanced Technology Microwave Sounder (ATMS) is one of the five key instruments onboard SNPP and is the heritage of Advanced Microwave Sounding Unit-A (AMSU-A) and Microwave Humidity Sounder (MHS) combined. AMSU-A and MHS are two crossing-scanning microwave radiometers onboard the past National Oceanic and Atmospheric Administration (NOAA) and European polar-orbiting satellites (e.g., NOAA-15, -16, -17, -18, -19, MetOp-A, -B). Compared with AMSU-A and MHS, ATMS has more channels, wider scan swath, overlapping field-of-view (FOV) sampling and higher spatial resolution temperature sounding channels than AMSU-A (Weng et al., 2012a). Soon after the launch of SNPP, ATMS on-orbit performance had been well characterized, channel noise and accuracy had exceeded the mission requirements, the ATMS data have been archived on NOAA's Comprehensive Large Array data Stewardship System (CLASS) and can be accessed by the broad user community.

Radiation at microwave frequencies emitted from atmospheric constituents such as oxygen allows for remote sensing of the atmospheric temperature. Through a two-point calibration equation (Mo, 1996; Zou et al., 2011), the signal from the microwave radiometer can be linked to the brightness temperature. In ATMS calibration, the biases are expected in radiance measurements due to many calibration error sources. For example, biases could also come from spacecraft emission, earth-view side lobe effects, and atmospheric inhomogeneity. The later often causes a scan-dependent bias feature for a cross-track scanning radiometer (Weng et al.,

2012b). It is important to quantify, document and correct these data biases before their applications in weather and climate predictions. This study investigates bias characteristics in ATMS data and proposes an absolute post-launch calibration algorithm using GPS RO data, which is SI-traceable.

Similar to satellite passive microwave instruments such as AMSU-A, calibrations of ATMS antenna brightness temperatures (TDR) data also lack the traceability to International Standard (SI) units. It is important to assess the instrument in-orbit accuracy for both NWP and climate applications. The Global Positioning System (GPS) Radio Occultation (RO) raw data are in principle SI traceable and have high accuracy and precision, high vertical resolution, no contamination from clouds, no system calibration required, and no instrument drift (Rocken et al. 1997; Anthes et al. 2000; Lin et al. 2010; Yang and Zou, 2012). In addition, the atmospheric radiative transfer models (RTMs) are very accurate for ATMS upper-troposphere and low stratosphere temperature sounding channels. These unique features of GPS ROs and RTMs make it possible to derive the in-orbit absolute calibration of ATMS upper-level temperature sounding channels 5-13. The CRTM simulations with GPS RO data as its input can be used for characterizing the statistical features of ATMS data from the post-launch in-orbit performance of the ATMS instrument.

An improved characterization of ATMS performance would also benefit the climate research using long-term climate data records (CDRs) consisting of observations from operational polar-orbiting satellite systems. ATMS inherited most of the sounding channels from its heritage predecessors: Advanced Microwave Sounding Unit-A (AMSU-A) and Microwave Humidity Sounder (MHS) onboard NOAA-15, NOAA-16, NOAA-17, NOAA-18 and NOAA-19 and MetOp-A satellites since 1998, and all four channels of the Microwave Sounding Unit

(MSU) onboard the early NOAA satellites from Tiros-N through NOAA-14 from 1979 to 2007. Therefore, there are nearly 35 years of four MSU channels global satellite data. MSU/AMSU-A brightness temperature observations were widely used by the community for climate studies (Christy *et al.*, 1998, 2000, 2003; Mears *et al.*, 2003, Mears and Wentz, 2009; Vinnikov and Grody, 2007; and Zou *et al.*, 2009). With ATMS onboard Suomi NPP, the MSU/AMSU time series can be further extended. Since a much more refined post-launch calibration is required to deduce long-term climate trend with adequate accuracy, precision, stability and consistency (Ohring *et al.*, 2005), this study could also contribute to future integration of ATMS data into long-term satellite CDRs.

As the first step of an in-orbit absolute calibration of ATMS data, this study aims at assessing the bias for ATMS upper level sounding channels using collocated GPS RO data. Sections 2-4 will briefly discuss the ATMS instrument characteristics, the Constellation Observing System for Meteorology, Ionosphere, and Climate/Formosa Satellite Mission 3 (COSMIC/FORMOSAT3, hereafter referred to as COSMIC for brevity) RO data, and the radiative transfer models used in this study. Section 5 discusses the collocation method. ATMS upper level sounding channel biases are estimated in Section 6 using fast radiative transfer model. Section 7 compares accuracy of the line-by-line ATMS brightness temperature simulations using laboratory-measured and BoxCar-approximated spectral response functions. Summary and conclusions are provided in Section 8.

## **2. A Brief Description of ATMS Instrument**

The carrier of ATMS, Suomi NPP, is rotating around the Earth on a circular,  $98.7^\circ$  inclination orbit at 824-km altitude. ATMS is a total-power, 22 channel passive microwave sounder with the scan angular span of  $\pm 52.77^\circ$  relative to nadir. A total of 96 field-of-view

(FOV) samples are taken along each scan line, and each FOV sample represents the mid-point of a sampling interval of about 18ms. Two receiving antennas are installed on the ATMS sensor, one is for channels 1-15 with frequencies below 60 GHz and the other is for channels 16-22 with frequencies above 60 GHz. The beam width is  $5.2^\circ$  for channels 1-2,  $2.2^\circ$  for channels 3-16 and  $1.1^\circ$  for channels 17-22 (Table 1). ATMS provides both temperature soundings within the surface to the upper stratosphere (about 1hPa,  $\sim 45\text{km}$ ), and humidity soundings within the surface to upper troposphere (about 200hPa,  $\sim 15\text{km}$ ).

The antenna reflectors continuously rotate counter-clockwise relative to the spacecraft direction of motion, completing three revolutions in eight seconds. Each scan cycle is divided into three segments. In the first segment, the Earth is viewed at 96 different angles, symmetric around the nadir direction. The angular range between the first and the last sample centroids is  $105.45^\circ$ . The antenna then accelerates and moves to a position that points toward an unobstructed space view (i.e., between the Earth's limb and the spacecraft horizon). It then resumes the same scan speed as maintained across the Earth scenes while four consecutive cold calibration measurements are taken. Next, the antenna is accelerated to move toward the zenith direction, points toward an internal calibration target that is at the relatively high ambient instrument temperature, and resumes the normal scan speed while four consecutive warm calibration measurements are taken. Finally, it is accelerated to the starting position viewing the Earth scene, where it is slowed down to normal scan speed to begin another scan cycle.

### **3. A Brief Description of COSMIC RO Data**

The GPS RO is a limb-sounding technique that makes use of radio signals emitted from the GPS satellites for sounding Earth's atmosphere. Under the assumption of the spherical symmetry of the atmospheric refractive index, vertical profiles of bending angle and refractivity can be

derived from the raw RO measurements of the excess Doppler shift of the radio signals transmitted by GPS satellites (see Appendix A1 in Zou et al. 1999). The profiles of refractivity are then used to generate profiles of the temperature and water vapor retrieval using a one-dimensional variational data assimilation (1D-Var) algorithm (Healy and Eyre, 2000; Palmer et al. 2000). The CDAAC wet retrieval is used in this study. A brief description of a 1D-Var algorithm for GPS RO retrieval is provided at <http://cosmic-io.cosmic.ucar.edu/cdaac/doc/documents/1dvar.pdf>.

The COSMIC satellite system consists of a constellation of six low-Earth-orbit (LEO) microsattellites, and was launched on April 15, 2006. Each LEO follows a circular orbit 512 km above the Earth surface, with an inclination angle of  $72^\circ$ . Currently, there are about 1000 soundings daily. The vertical resolution is 0.1km from surface to 39.9 km, and each GPS RO measurement quantifies an integrated atmospheric refraction effect over a few hundred kilometers along a ray path centered at the tangent point. The global mean differences between COSMIC and high-quality reanalysis within the height range between 8 and 30 km are estimated to be  $\sim 0.65\text{K}$  (Kishore et al. 2008). The precision of COSMIC GPS RO soundings, estimated by comparison of closely collocated COSMIC soundings, is approximately 0.05K in the upper troposphere and lower stratosphere (Anthes et al. 2008). In the water vapor abundant region in the lower troposphere (e.g., when temperature is greater than 270K), the precision reduces to about 0.1K. In the ionosphere regions, GPS profiles become less accurate due to residual ionospheric effect. The estimated precision of COSMIC GPS RO soundings is approximately 0.2K in the ionosphere.

## **4. Radiative Transfer Models**

### **4.1 CRTM**

CRTM stands for Community Radiative Transfer Model and is developed and distributed by the US Joint Center for Satellite Data Assimilation (JCSDA). The model is publicly available and may be downloaded from <ftp://ftp.emc.ncep.noaa.gov/jcsda/CRTM/REL-2.0.5/>. The CRTM is a sensor-channel-based radiative transfer model (Han et al. 2006; Weng et al. 2007; Han et al. 2010) and is widely used for microwave and infrared satellite data assimilation and remote sensing applications. It includes modules that compute the satellite-measured thermal radiation from gaseous absorption, absorption and scattering of radiation by aerosols and clouds, and emission and reflection of radiation by the Earth surface. The input to the CRTM includes atmospheric state variables (temperature, water vapor, pressure, and ozone concentration at user defined layers, and optionally, liquid water content and mean particle size profiles for up to six cloud types), and surface state variables and parameters including the surface emissivity, surface skin temperature, and surface wind. In addition to CRTM (i.e., the forward model), the corresponding tangent-linear, adjoint, and K-matrix models have also been included in the CRTM package.

In this study, the vertical profiles of temperature, water vapor and pressure are obtained directly from COSMIC GPS RO retrieval. The mixing ratio profile of ozone is set to be equal to the U.S. standard atmospheric state. For simplicity, no cloud or aerosols are considered in the radiative transfer simulation. The emissivity is derived from the CRTM oceanic surface model at microwave frequencies.

## **4.2 MonoRTM**

The Atmospheric and Environmental Research (AER) Inc. Monochromatic Radiative Transfer Model (MonoRTM) is an accurate line-by-line RTM for use in the microwave region. It employs an accurate atmospheric spectroscopy database and only considers gaseous absorption.

A detailed description of MonoRTM physics can be found in Clough et al. (2005) and Payne et al. (2011). Figure 1 shows the amount of contributions of different atmospheric constituents in the microwave region, which is calculated using MonoRTM for a U.S. standard atmosphere. Between 50-70 GHz, O<sub>2</sub> is the only absorption gas. By including the fine absorption line (Fig. 1b), MonoRTM accurately simulates the ATMS microwave sounding channels within 50-70 GHz O<sub>2</sub> absorption band through a line-by-line calculation procedure. In this study, MonoRTM version 4.2 is used. Input to MonoRTM is the same as that for CRTM, i.e., the vertical profiles of temperature, water vapor and pressure from COSMIC GPS RO retrieval.

## **5. Collocation between GPS RO and ATMS**

In the present study, COSMIC RO soundings collocated with ATMS measurements are selected for assessing the accuracy of ATMS measurements. The collocation criteria are set by a time difference of no more than three hours and a horizontal spatial separation of less than 50 km at the altitude of peak weight function. If there are more than one ATMS pixel measurements satisfying these collocation criteria, the one that is closest to the related COSMIC sounding is chosen and others are discarded. Because surface state variables and parameters are not provided by COSMIC ROs, only upper-level temperature sounding channels are simulated using COSMIC GPS RO data. The NCEP GFS surface wind field is used in the forward model calculations. The surface emission variation due to changes in wind speed could contribute to the simulation of ATMS channel 5. The global biases as well as the angular dependence of biases are estimated.

As the GPS radio signal passes through the atmosphere, its ray path is bent over due to variations of atmospheric refraction. Therefore, the geolocation of the perigee point (also called tangent point) of a single RO profile varies with altitude. On the other hand, a satellite measurement at a specific frequency represents a weighted average of radiation emitted from

different layers of the atmosphere. The magnitude of such a weighting is determined by a channel-dependent weighting function (WF). The measured radiation is most sensitive to the atmospheric temperature at the altitude where the WF reaches a maximum. The WF also varies with scan angle (Fig. 2). For each channel, the altitude of the peak WF is the lowest at the nadir and increases with the scan angle. Considering the geolocation change of the perigee point of a GPS RO profile with altitude, the geolocation of a GPS RO at the altitude where the WF for each collocated ATMS FOV of a particular sounding channel reaches the maximum is used for implementing the spatial collocation criteria of less than 50 km, where the altitude of the maximum WF is determined by inputting the U.S. standard atmosphere into CRTM (see Table 1).

Based on the fact that the surface emissivity influences vary greatly over land, and the physical properties of brightness temperature for the sounding channels are affected by clouds, a cloud detection algorithm similar to Weng et al. (2003) is applied to separate the data in clear-sky conditions over ocean from total ATMS measurements (Weng et al., 2012a). Figure 3a presents the spatial distribution of the ATMS observations that are collocated with COSMIC GPS RO data in clear-sky conditions over ocean and between 60S-60N from December 10, 2011 to June 30, 2012. Most collocated data are located in subtropical in Northern Hemisphere and middle latitudes in Southern Hemisphere, which is largely determined by the latitudinal dependence of the ocean area (Fig. 3b). A similar pattern is found for channels 5, 7-13.

## **6. Bias Estimate and GPS RO Calibration Results**

For brevity, model simulations of the ATMS brightness temperatures using GPS RO profiles as input to CRTM will be denoted  $B^{\text{GPS}}$  hereafter. The altitudes of the maximum WF of ATMS channels 14-15 are above 40 km, which is the top of COSMIC RO data. Therefore, biases of

ATMS channels 14-15 are not included in this study. Figure 4 presents scatter plots of brightness temperature from ATMS observations (O) and GPS RO simulations ( $B^{\text{GPS}}$ ) for all collocated data points under clear-sky conditions over ocean between 60S-60N from December 10, 2011 to June 30, 2012. In general, CRTM simulations with GPS RO input profiles correlate quite well with ATMS observations. A noticeable temperature dependence of the differences ( $O-B^{\text{GPS}}$ ) between observations and simulations is seen in channel 6. Global biases estimated by the mean differences ( $O-B^{\text{GPS}}$ ) are positive for channels 6, 10-13 with values smaller than 0.5K and negative for channels 5, 7-9 with values greater than -0.7K (Fig. 5). The standard deviation is smallest for channel 8 ( $\sim 0.25\text{K}$ ), increases with channel number to about 2.0K at channel 13 (Fig. 5). The standard deviations for channels 5 and 6 are 0.4K and 0.6K, respectively.

A strong latitudinal dependence of global biases is found for ATMS data (Fig. 6a). Positive biased for channels 5-6, 10-13 are largest in low latitudes. A weaker latitudinal dependence of biases is found for ATMS channels 7-9 (Fig. 6a). The standard deviations (Fig. 6b) have a smaller latitudinal dependence than biases.

For a cross-track scanning radiometer like ATMS, the variation of the optical path length with scan angle is modeled through CRTM. However, the variation of atmospheric inhomogeneity with scan angle has not been explicitly simulated in CRTM. In addition, effects of the spacecraft radiation on brightness temperatures can also vary with scan angle. Therefore, a scan-angle dependent bias is expected for the cross-track scanning radiometer. In many applications such as weather predictions through radiance data assimilation, angular-dependent biases must be properly quantified so that they could be removed before data applications.

Figure 7 presents scan-dependent biases and standard deviations of ATMS channels 5-13 estimated by using GPS RO data. Variations of GPS RO profiles numbers collocated with

ATMS data are also shown in Fig. 7. As expected, the total number of collocated GPS ROs increases with scan angle since the size of FOV increases with scan angle. An asymmetric scan bias pattern is noticed for ATMS channels 5-10. ATMS temperature sounding channels are more negatively biased near the ends of ATMS scan lines. The standard deviations of ATMS channels 6, 12 and 13 are much larger than the remaining channels. The root causes of the asymmetric bias pattern came from the contributions from the near field (e.g., spacecraft) side-lobes, which were confirmed by using the ATMS pitch maneuver data (Weng et al., 2012b). The closer the spacecraft temperature is to a channel's temperature, the less impact of the spacecraft side-lobes on the scan bias of that channel.

Spatial distributions of the differences of brightness temperature between ATMS observations and GPS RO simulations ( $O-B^{GPS}$ ) after the GPS RO absolute post-launch calibration are much more homogeneously distributed over the globe than those without the GPS RO absolute post-launch calibration. Figure 8a-b presents frequency distributions of  $O-B^{GPS}$  differences before and after the GPS RO absolute post-launch calibration are plotted for ATMS channels 5-13 using all collocated data from December 10, 2011 to June 30, 2012 under clear-sky conditions over ocean within 60S-60N. Monthly variations of biases and standard deviations of the differences between ATMS observations and GPS RO simulations ( $O-B^{GPS}$ ) after the GPS RO absolute post-launch calibration are provided in Fig. 8c. A noticeable difference of the frequency distribution between Figs. 8a and 8b is in the variation of bias with channel number. Before GPS RO calibration, the biases with different channels are different. After GPS RO calibration, all channels assume a nearly normal Gaussian distribution. The only differences among different channels are the standard deviations. By comparing Fig. 8c with Fig. 5, it is seen that global biases after the GPS RO calibration are about an order of magnitude smaller than

those of the original TDR data. Impacts of GPS RO calibration on the standard deviations are only slightly reduced. The standard deviations increase fast for upper-level channels 10-13 in a similar way as their noise equivalent temperature difference (NEDT) values (see Table 1). The standard deviations for these channels after GPS calibration (Fig. 8) are only slightly larger than their NEDT values.

Another noticeable feature from Fig. 8 is that the width of the Gaussian frequency distribution for an individual channel is reduced after the GPS RO calibration. This is due to the fact that data from all FOVs are plotted in Fig. 8 while biases for a cross-track microwave instrument are FOV-dependent. If the Gaussian frequency distribution for a specified FOV is plotted (Fig. 9), the width of the Gaussian frequency distribution for an individual channel does not change.

## **7. MonoRTM Simulations Using Measured and Boxcar Spectral Response Function**

In CRTM, the relative spectral response function (SRF) is set as Boxcar, i.e., the relative SRF uniformly set to equal to one between the band frequency boundaries. For each band, there are 256 absorption lines. More specifically, if there are two bands or four bands for a certain channel, the number of lines is 128 and 64 within the second and third sub-band. In March 2012, the ATMS Pre-Flight Model (PFM) SRF report is provided by Kim and Lyu (2012), in which the PFM filter digitized SRF data at three base-plate temperatures (-10°C, +20°C and +50°C) and at low, nominal and high oscillator bias levels are presented. For V, W and G bands, the laboratory experiments were performed for both primary and secondary local oscillator settings.

With the above-mentioned laboratory-measured SRF, the accuracy of CRTM can be assessed using the MonoRTM. The top level of the COSMIC GPS RO data is extended from about 2hPa to 0.005hPa using 1976 US standard atmospheric profile. To save computational

time, the SRF is truncated at -20dB to keep the 99% of the maximum SRF for each band of each channel. Details of the relative SRF before and after the truncations are listed in Table 2. Compared to 256 lines for Boxcar SRF, the number of lines for truncated measured SRF is at least tripled for each channel. The ATMS Boxcar and -20dB truncated relative SRF for each channel are shown in Fig. 10. It is found that the ATMS Boxcar frequency boundary generally matches with the -20dB truncated SRF quite well for ATMS channels 5-13. The global biases and standard deviations of the MonoRTM-simulated brightness temperature differences between the Boxcar and the -20dB-truncated SRF in January 2012 are shown in Fig. 11. We can see the mean difference is within  $\pm 0.2\text{K}$  for all channels, which is larger than the data biases after GPS RO post-launch calibration (Fig. 8c). The standard deviations are also less than 0.2K, which is an order of magnitude smaller than the standard deviations of  $O-B^{\text{GPS}}$ . It is thus concluded that for NWP radiance data assimilation, the forward radiative transfer models should either use the measured SRFs or remove model biases introduced by using the Boxcar SRF estimated in Fig. 11.

## 8. Summary and Conclusions

GPS RO observations are very accurate from 2-3 km to about 40 km and are most accurate between 8 and 30 km, making them ideally suitable for estimating biases of upper level ATMS temperature sounding channels. In the past seven months from December 10, 2011 to June 30, 2012, COSMIC GPS RO data and ATMS upper-level sounding observations are collocated. Since the geographical location of a single GPS RO profile could vary for more than a few hundred kilometers from the top of the atmosphere to the observed lowest altitude, the collocation between a COSMIC GPS RO profile and a FOV of an ATMS channel is carried out between the geographical location of both types of data at the ATMS channel peak weighting

function altitude. Statistical features of the differences between ATMS observations and GPS RO simulations for upper-level sounding channels are analyzed using all collocated data under clear-sky conditions over ocean. The GPS RO simulations are produced by CRTM. Since the proposed absolute post-launch calibration of ATMS satellite measurements using GPS RO data relies on CRTM, the model bias of CRTM is estimated. Specifically, biases of different ATMS channels using the so-called Boxcar SRF that is implemented in CRTM is assessed using an accurate line-by-line radiative transfer model (e.g., MonoRTM). Comparison of simulations obtained from using the measured SRF versus the Boxcar SRF shows a CRTM model bias less than  $\pm 0.2\text{K}$ . The largest model bias of about  $0.18\text{K}$  occurred in ATMS channel 7.

The ATMS global brightness temperature biases are within  $\pm 0.7\text{K}$  for all channels examined (e.g., ATMS channels 5-13). The magnitudes of biases vary with channel number. A small monthly variation of biases is observed. The error distributions are not of normal Gaussian types. Also, the biases have an asymmetric distribution with respect to scan angle. When such an asymmetric scan-dependent bias estimated by GPS RO simulation for each individual channel is removed from the data, the errors of the ATMS sensor data record (SDR) at channels 5-13 becomes a normal Gaussian distribution.

The present study will contribute to the establishment of satellite microwave temperature sounding climate data record which requires the ATMS data be linked to earlier NOAA polar-orbiting satellite microwave temperature sounding data (e.g., MSU and AMSU-A). It is noted that the temperature and water vapor profiles retrieved by a 1D-Var approach could have some dependence on the first guess and the vertical error covariance matrix. We plan to quantify such a dependence, and if necessary, to rerun all GPS RO 1D-Var experiments in the future study [for the proposed calibration of ATMS upper level temperature sounding channels.](#)

***Disclaimer and Acknowledgements:*** The views expressed in this publication are those of the authors and do not necessarily represent those of NOAA. The first author is supported by Chinese Ministry of Science and Technology project 2010CB951600.

## REFERENCES

- Anthes, R.A., C. Rocken, and Y. H. Kuo, 2000: Applications of COSMIC to meteorology and climate. *TAO*, **11**, 115-156.
- , and Coauthors, 2008: The COSMIC/FORMOSAT-3 mission: Early results. *Bull. Amer. Meteor. Soc.*, **89**, 313-333.
- Christy, J.R., R.W. Spencer, and E.S. Lobl, 1998: Analysis of the merging procedure for the MSU daily temperature time series. *J. Climate*, **11**, 2016-2041.
- , and W.D. Braswell, 2000: MSU tropospheric temperatures: Dataset construction and radiosonde comparisons. *J. Atmos. Oceanic Technol.*, **17**, 1153-1170.
- , W.B. Norris, W.D. Braswell, and D.E. Parker, 2003: Error estimates of version 5.0 of MSU-AMSU bulk atmospheric temperatures. *J. Atmos. Oceanic Technol.*, **20**, 613-629.
- Clough, S.A., M.W. Shephard, E.J. Mlawer, J.S. Delamere, M. Iacono, K.E. Cady-Pereira, S. Boukabara and P.D. Brown, 2005: Atmospheric radiative transfer modeling: A summary of the AER codes, *JQSRT*, **91**, no.2, 233-244.
- Hajj, G.A., and Coauthors, 2004: CHAMP and SAC-C atmospheric occultation results and intercomparisons. *J. Geophys. Res.*, **109**, D06109, doi: 10.1029/2003JD003909.
- Han, Y., P. van Delst, Q. Liu, F. Weng, B. Yan, R. Treadon, and J. Derber, 2006: JCSDA community radiative transfer model (CRTM)—version 1. NOAA Tech. Rep., NESDIS 122, 40pp.
- , -----, F. Weng, Q. Liu, D. Groff, B. Yan, Y. Chen, and R. Vogel, 2010: Current status of the JCSDA community radiative transfer model (CRTM). *17th Int. ATOVS Study Conf.*, Monterey, CA, U.S.A., World Meteorological Organization.

- Healy, S., and J. Eyre, 2000: Retrieving temperature, water vapor and surface pressure information from refractivity-index profiles derived by radio occultation: A simulation study. *Quart. J. Roy. Meteor. Soc.*, **126**, 1661-1683.
- Kim, E, and Lyu, C.-H.J., 2012: Readme information for the NPP ATMS spectral response function (SRF) dataset for public release.
- Kishore, P. S. P. Namboothiri, J. H. Jiang, V. Sivakumar, and K. Igarashi, 2008: Global temperature estimates in the troposphere and stratosphere: A validation study of COSMIC/FORMOSAT-3 measurements. *Atmos. Chem. Phys. Discuss.*, **8**, 8327-8355.
- Lin, L., X. Zou and Y-H. Kuo, 2010: COSMIC GPS radio occultation temperature profiles in clouds. *Mon. Wea. Rev.*, **138** (4), 1104-1118.
- Mears, C. A., and F.J. Wents, 2009: Construction of the Remote Sensing Systems V3.2 atmospheric temperature records from the MSU and AMSU Microwave Sounders. *J. Atmos. Oceanic Technol.*, **26**, 1040-1056.
- , M. C. Schabel, and F.J. Wents, 2003: A reanalysis of the MSU channel 2 tropospheric temperature record. *J. Climate*, **16**, 3650-3664.
- Mo, T., 1996: Prelaunch Calibration of the Advanced Microwave Sounding Unit-A for NOAA-K. *IEEE Transaction on Microwave Theory and Techniques*, **44**, 1460-1469.
- National Polar-Orbiting Operational Environmental Satellite System (NPOESS) Advanced Technology Microwave Sounder (ATMS) SDR Radiometric Calibration Algorithm Theoretical Basis Document (ATBD) (D43751 Rev C), CDRL No. A032.
- Ohring G., B. Wielicki, R. Spencer, B. Emery, and R. Dalta, 2005: Satellite instrument calibration for measuring global climate change. *Bull. Amer. Meteor. Soc.*, **86**, 1303-1313.

- Palmer, P. I., J. Barnett, J. Eyre, and S. Healy, 2000: A non-linear optimal estimation inverse method for radio occultation measurements of temperature, humidity, and surface pressure. *J. Geophys. Res.*, **105**, 17513-17526.
- Payne, V.H., E.J. Mlawer, K.E. Cady-Pereira and J-L. Moncet, 2011: Water vapor continuum absorption in the microwave. *IEEE Trans. Geosci. Remote Sens.*, **49**, No.6, doi:10.1109/TGRS. 2010.2091416.
- Rocken, C., and Coauthors, 1997: Analysis and validation of GPS/MET data in the neutral atmosphere. *J. Geophys. Res.*, **102**, 29849-29866.
- Vinnikov, K. Y., and N. C. Grody, 2003: Global warming trend of mean tropospheric temperature observed by satellites. *Science*, **302**, 269-272.
- Weng, F., L. Zhao, R. Ferraro, G. Poe, X. Li, and N. Grody, 2003: Advanced Microwave Sounding Unit Cloud and Precipitation Algorithms. *Radio Sci.*, **38**, 8,086-8,096, doi:10.1029/2002RS002679.
- , 2007: Advances in radiative transfer modeling in support of satellite data assimilation, *J. Atmos. Sci.*, **64**, 3803,3811.
- , X. Zou, X. Wang, S. Yang, M. Goldberg, 2012a: Introduction to Suomi NPP ATMS for NWP and Tropical Cyclone Applications, *J. Geophys. Res.*, doi:10.1029/2012JD018144
- , H. Yang, X. Zou, 2012b: On Convertibility from Antenna to Sensor Brightness Temperature for Advanced Technology Microwave Sounder (ATMS), *IEEE Geosci. Remote Sens. Lett.*, (Accepted).
- Zou, X., F. Vandenberghe, B. Wang, M. E. Gorbunov, Y.-H. Kuo, S. Sokolovskiy, J. C. Chang, J. G. Sela, and R. Anthes, and Coauthors, 1999: A ray-tracing operator and its adjoint for the use of GPS/MET refraction angle measurements. *J. Geophys. Res.*, **104**(D18), 22301-22318.

Zou, X., X. Wang, F. Weng and G. Li, 2011: Assessments of Chinese FengYun Microwave Temperature Sounder (MWTS) measurements for weather and climate applications. *J. Ocean Atmos. Tech.*, **28**, 1206-1227.

Zou, C., M. Gao, and M.D. Goldberg, 2009: Error structure and atmospheric temperature trends in observations from the Microwave Sounding Unit. *J. Climate*, **22**, 1661-1681.

## Table Caption

Table 1: ATMS channel characteristics (e.g., channel number, central frequency, beamwidth, NE $\Delta$ T) and the peak weighting function height calculated for U.S. standard atmosphere.

For brevity,  $f_0=57.2903$ .

Table 2: Total number of absorption lines used in the ATMS SRFs before and after the -20dB truncation.

## Figure Caption

Fig. 1: (a) Total optical depth between 0-250 GHz calculated by the line-by-line radiative transfer model (MonoRTM) using the U.S. standard atmosphere (black). Contributions to the total optical depth from H<sub>2</sub>O, O<sub>2</sub>+N<sub>2</sub> and other gases are shown in blue, red and green, respectively. (b) Same as (a) except for the spectral range from 50-70 GHz highlighted in grey.

Fig. 2: Angular-dependence of ATMS weighting function profiles for ATMS channels 5-13 (shaded) calculated by CRTM using the U.S. standard atmospheric profile.

Fig. 3: (a) Spatial distribution of ATMS measurements that are collocated with COSMIC ROs in 2°x2° grid for Channel 6. The similar patterns are found for other channels. (b) Latitudinal distributions of the number of data points at 5° latitudinal band for all collocated soundings under clear-sky conditions over ocean and between 60S-60N from December 10, 2011 to June 30, 2012.

Fig. 4: Scatter plots of brightness temperature from ATMS observations and CRTM simulations with input from collocated COSMIC data under clear-sky over ocean between 60S-60N from December 10, 2011 to June 30, 2012.

Fig. 5: Biases (bar) and standard deviations (curve) of the differences between ATMS observations and GPS RO simulations ( $O-B^{GPS}$ ) calculated for all collocated data under clear-sky conditions over ocean and between 60S-60N from December 10, 2011 to June 30, 2012.

Fig. 6: Latitudinal distributions of (a) biases and (b) standard deviations calculated at  $5^\circ$  latitudinal interval for all collocated soundings under clear-sky conditions over ocean and between 60S-60N from December 10, 2011 to June 30, 2012.

Fig. 7: Angular-dependence of brightness temperature biases (solid curve) and standard deviations (shaded area) estimated by the differences between ATMS observations and GPS RO simulations ( $O-B^{\text{GPS}}$ ) for collocated data under-clear sky over ocean between 60S-60N. The GPS RO profiles numbers collocated with ATMS data are also shown (dashed curve).

Fig. 8: Frequency distributions of  $O-B^{\text{GPS}}$  differences for ATMS channels 5-13 before (a) and after (b) the GPS RO absolute post-launch calibration for all data from December 10, 2011 to June 30, 2012 under clear-sky conditions over ocean between 60S-60N. (c) Same as Fig. 5 except for the removal of the GPS RO derived scan bias.

Fig. 9: Frequency distribution of  $O-B^{\text{GPS}}$  differences for ATMS channels 5-13 (a)-(b) before and (c)-(d) after the GPS RO absolute post-launch calibration for FOV1 (left panels) and nadir FOV 48 (right panels) using all data from December 10, 2011 to June 30, 2012 under clear-sky conditions over ocean between 60S-60N.

Fig. 10: Laboratory-measured SRF used in line-by-line model after -20dB truncation (black line) and the boxcar SRF using in CRTM (shading) for ATMS channels 5-13.

Fig. 11: Global means (bar) and standard deviations (curve) of the differences between GPS RO simulated brightness temperatures using the -20dB truncated SRF and the Boxcar SRF for one month data in January 2012 under clear-sky conditions over ocean within 60S-60N.

Table 1: ATMS channel characteristics (e.g., channel number, central frequency, beamwidth, NE $\Delta$ T) and the peak weighting function height calculated for U.S. standard atmosphere.

For brevity,  $f_0=57.2903$ .

Channel	Central Frequency (GHz)	Beam Width (deg)	NE $\Delta$ T (K)	Peak WF (mb)
1	23.8	5.2	0.5	1085.394
2	31.4	5.2	0.6	1085.394
3	50.3	2.2	0.7	1085.394
4	51.76	2.2	0.5	1085.394
5	52.8	2.2	0.5	891.7679
6	$53.596 \pm 0.115$	2.2	0.5	606.847
7	54.4	2.2	0.5	351.237
8	54.94	2.2	0.5	253.637
9	55.5	2.2	0.5	165.241
10	$f_0$	2.2	0.75	86.337
11	$f_0 \pm 0.217$	2.2	1.0	49.326
12	$f_0 \pm 0.322 \pm 0.048$	2.2	1.0	24.793
13	$f_0 \pm 0.322 \pm 0.022$	2.2	1.5	10.240
14	$f_0 \pm 0.322 \pm 0.010$	2.2	2.2	5.385
15	$f_0 \pm 0.322 \pm 0.004$	2.2	3.6	3.010
16	88.2	2.2	0.3	1085.394
17	165.5	1.1	0.6	1085.394
18	$183.31 \pm 7$	1.1	0.8	790.017
19	$183.31 \pm 4.5$	1.1	0.8	695.847
20	$183.31 \pm 3$	1.1	0.8	606.847
21	$183.31 \pm 1.8$	1.1	0.8	506.115
22	$183.31 \pm 1$	1.1	0.9	450.738

Table 2: Total number of absorption lines used in the ATMS SRFs before and after the -20dB truncation.

Channel	Total number of absorption line	Total number of truncated absorption line	Averaged spectral Resolution (MHz)
1	2501	937	0.3200
2	1601	651	0.3125
3	1001	694	0.3000
4	1001	716	0.6000
5	1001	664	0.6000
6	2002	1188	0.3000
7	1001	708	0.6000
8	1001	705	0.6000
9	1001	690	0.5000
10	2002	1788	0.1850
11	2002	1422	0.1250
12	2002	982	0.1650
13	2002	1004	0.0750
14	2002	1204	0.0350
15	2002	922	0.0164
16	1600	1114	1.8750
17	2002	1450	1.7000
18	2002	1408	2.9670
19	2002	1214	3.4600
20	2002	1102	1.9780
21	2002	1088	1.9740
22	2002	1396	0.7900
Total	37,734	23,047	

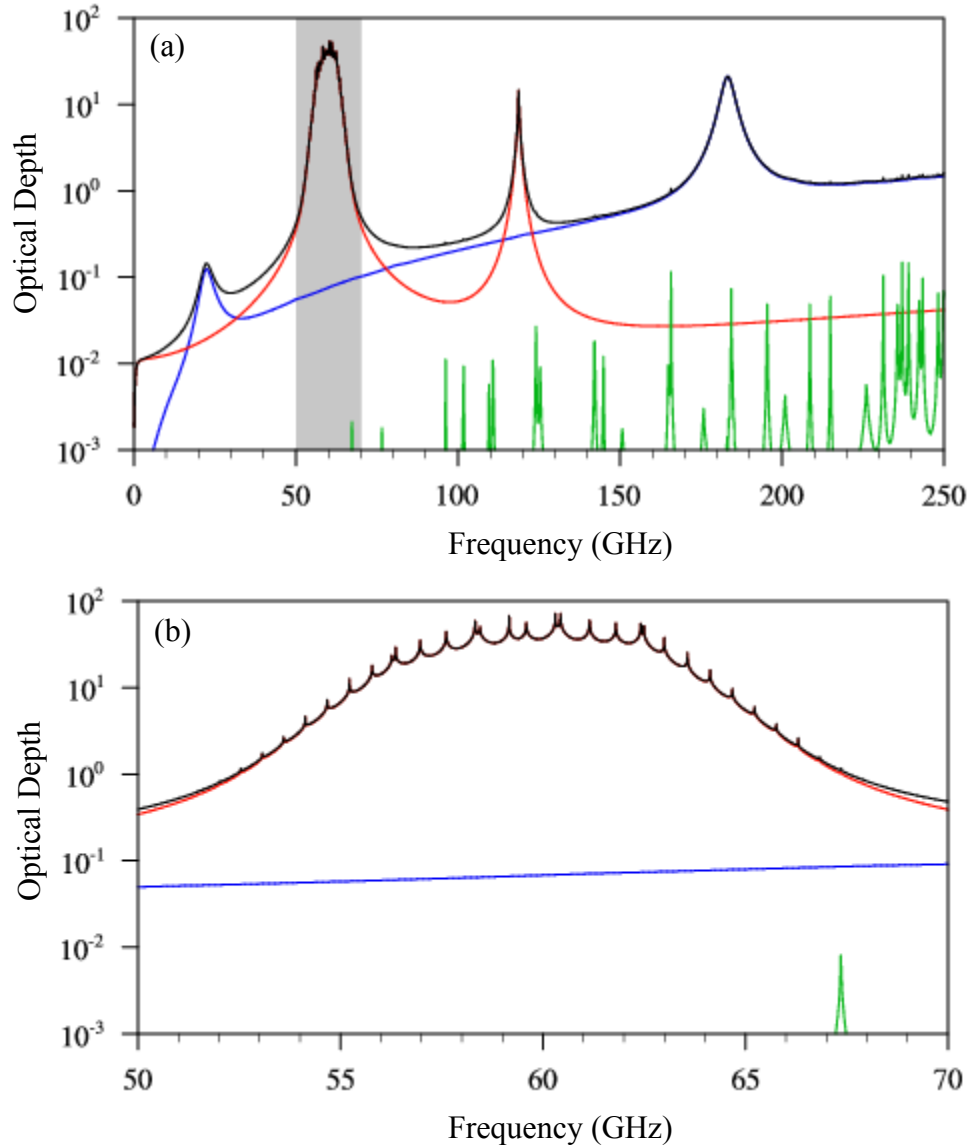
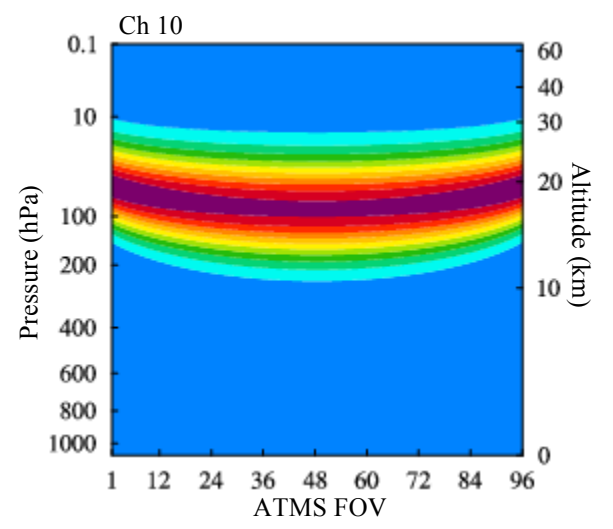
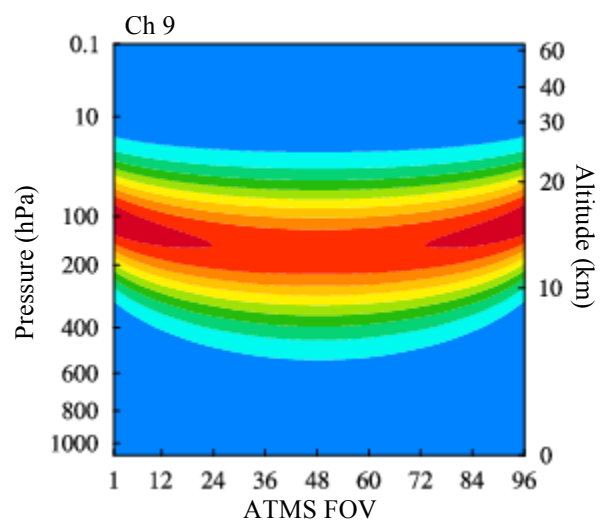
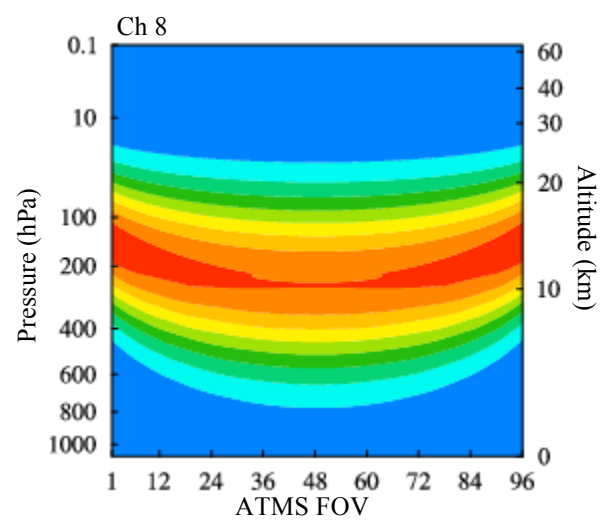
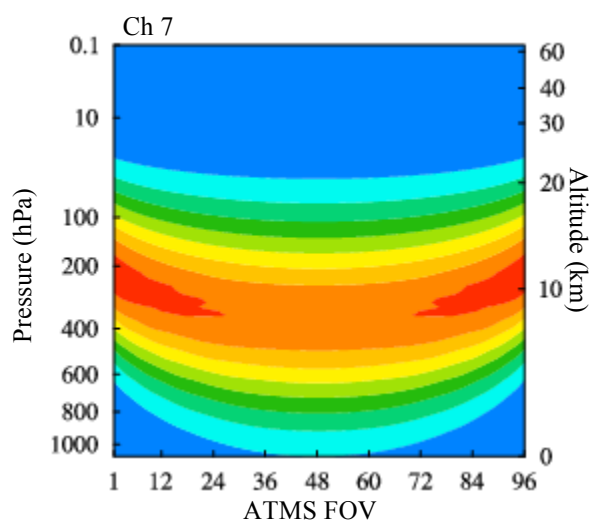
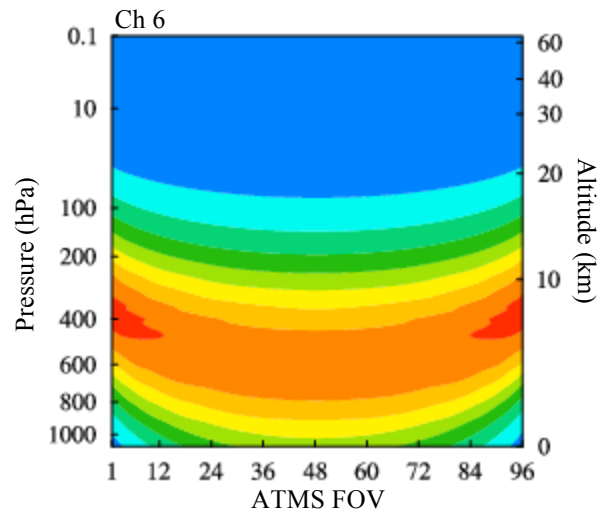
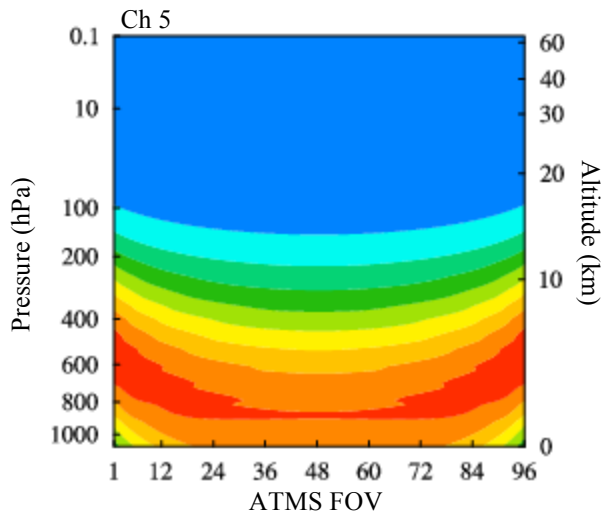


Fig. 1: (a) Total optical depth between 0-250 GHz calculated by the line-by-line radiative transfer model (MonoRTM) using the U.S. standard atmosphere (black). Contributions to the total optical depth from  $H_2O$ ,  $O_2+N_2$  and other gases are shown in blue, red and green, respectively. (b) Same as (a) except for the spectral range from 50-70 GHz highlighted in grey.



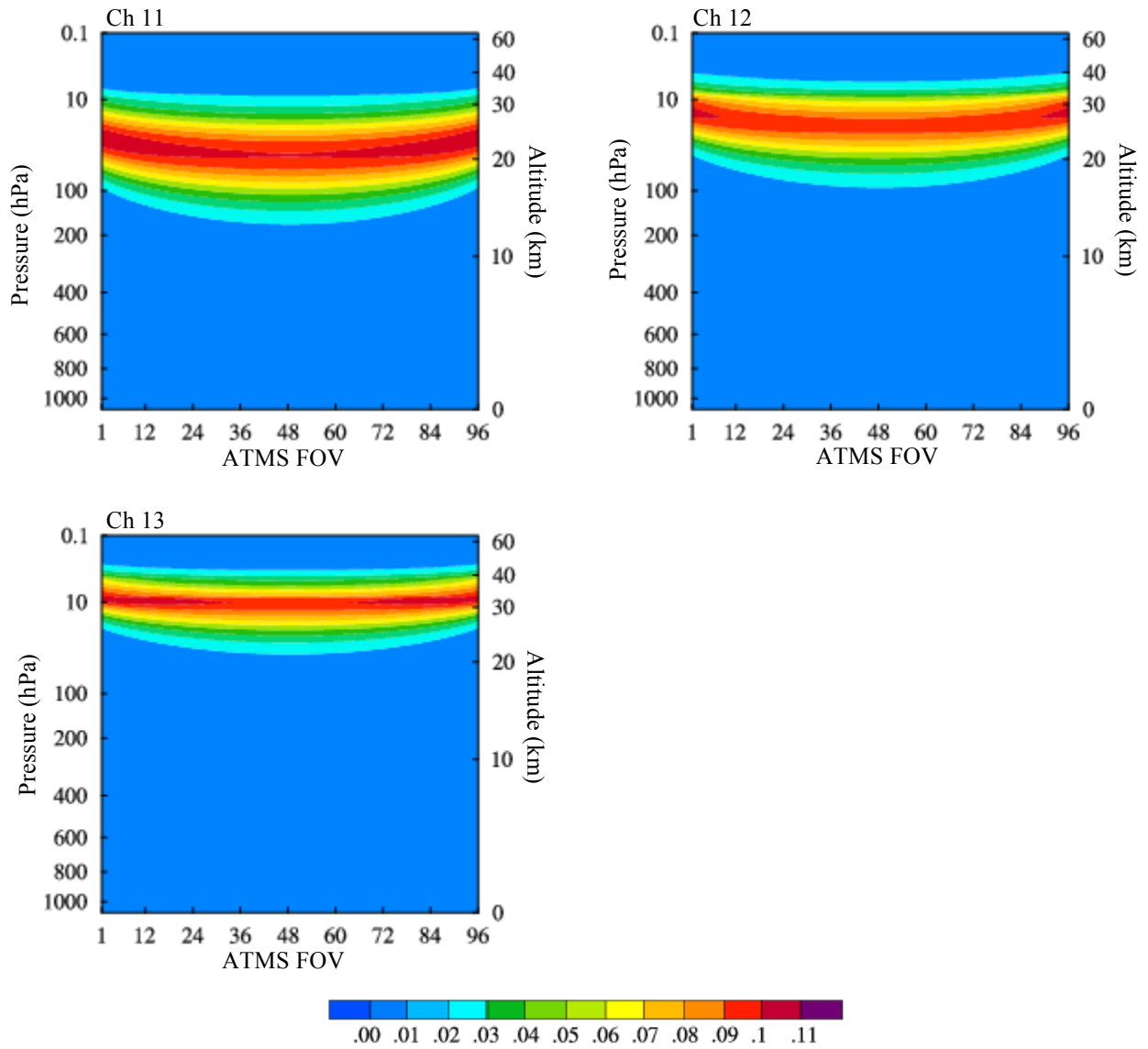


Fig. 2: Angular-dependence of ATMS weighting function profiles for ATMS channels 5-13 (shaded) calculated by CRTM using the U.S. standard atmospheric profile.

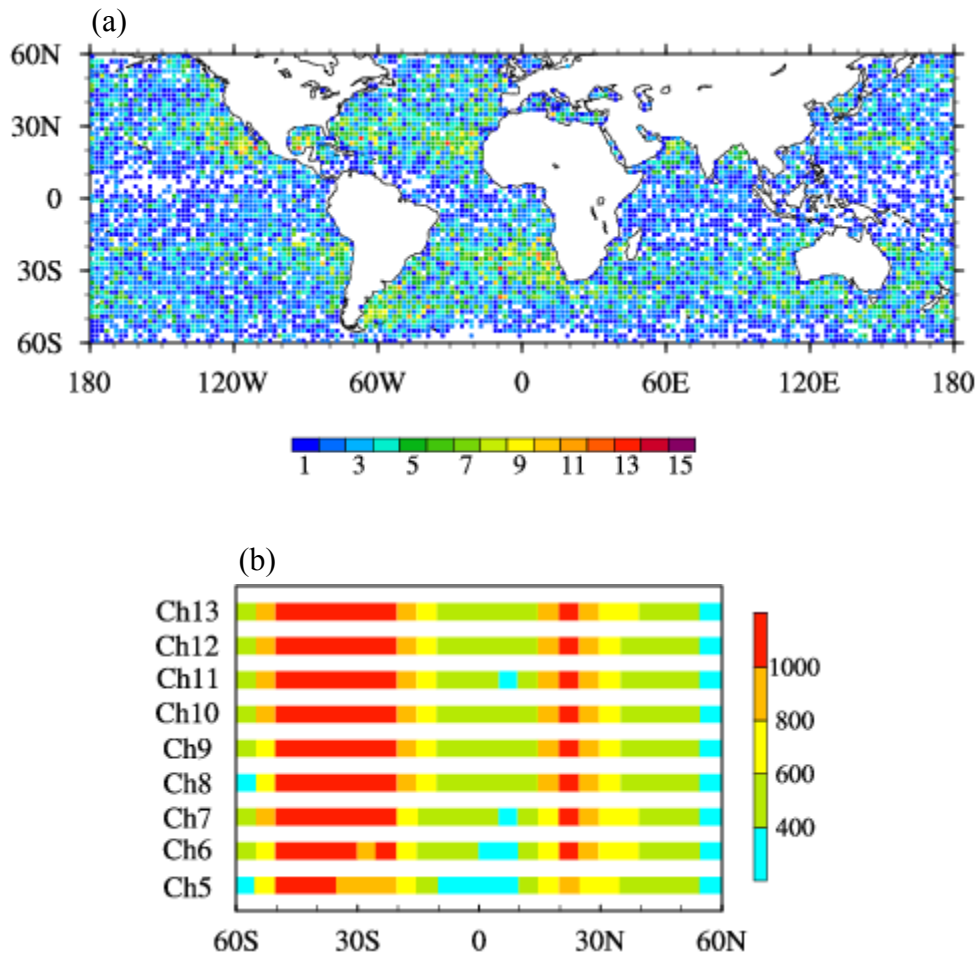
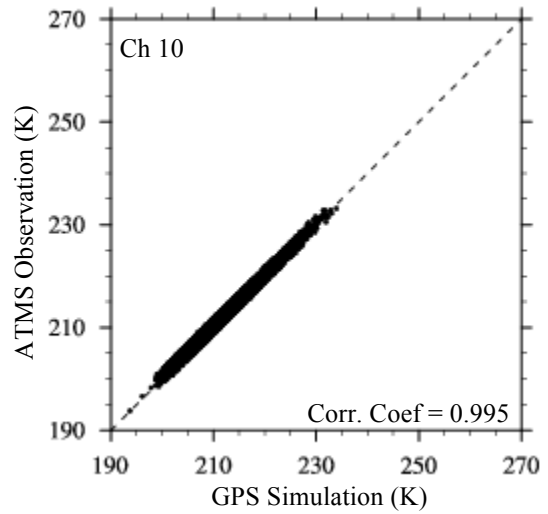
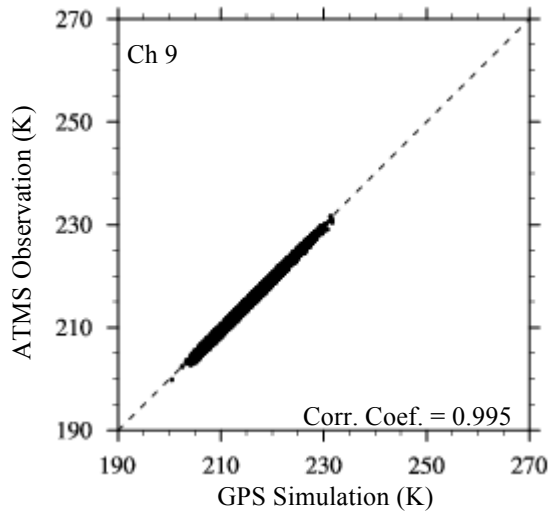
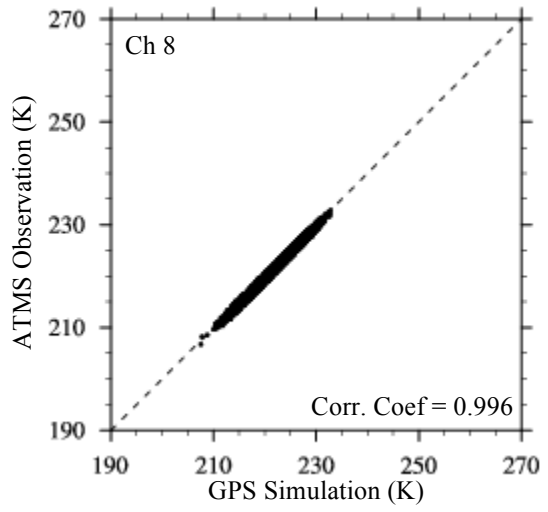
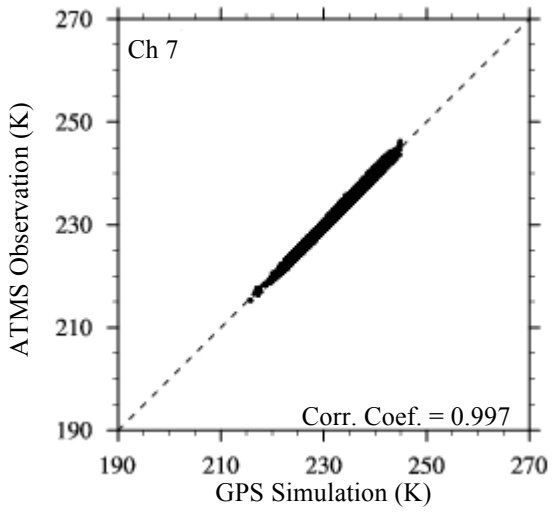
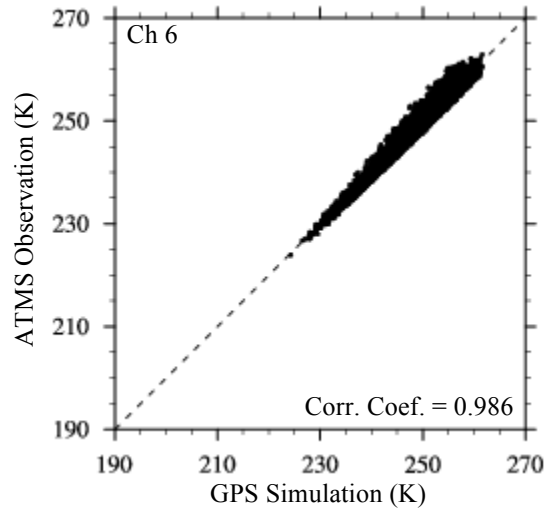
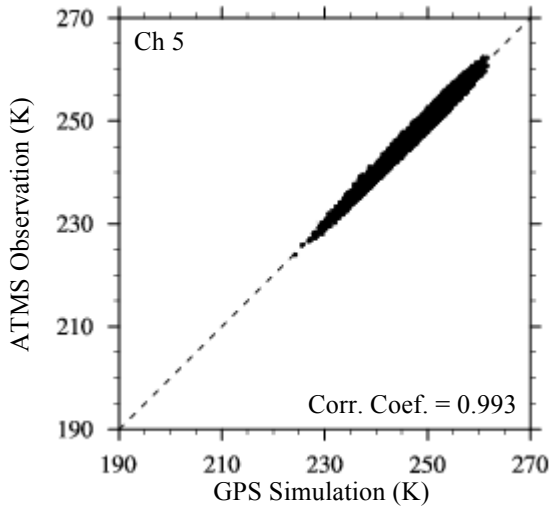


Fig. 3: (a) Spatial distribution of ATMS data counts that are collocated with COSMIC ROs in  $2^\circ \times 2^\circ$  grid for Channel 6. The similar patterns are found for other channels. (b) Latitudinal distributions of the number of data points at  $5^\circ$  latitudinal band for all collocated soundings under clear-sky conditions over ocean and between 60S-60N from December 10, 2011 to June 30, 2012.



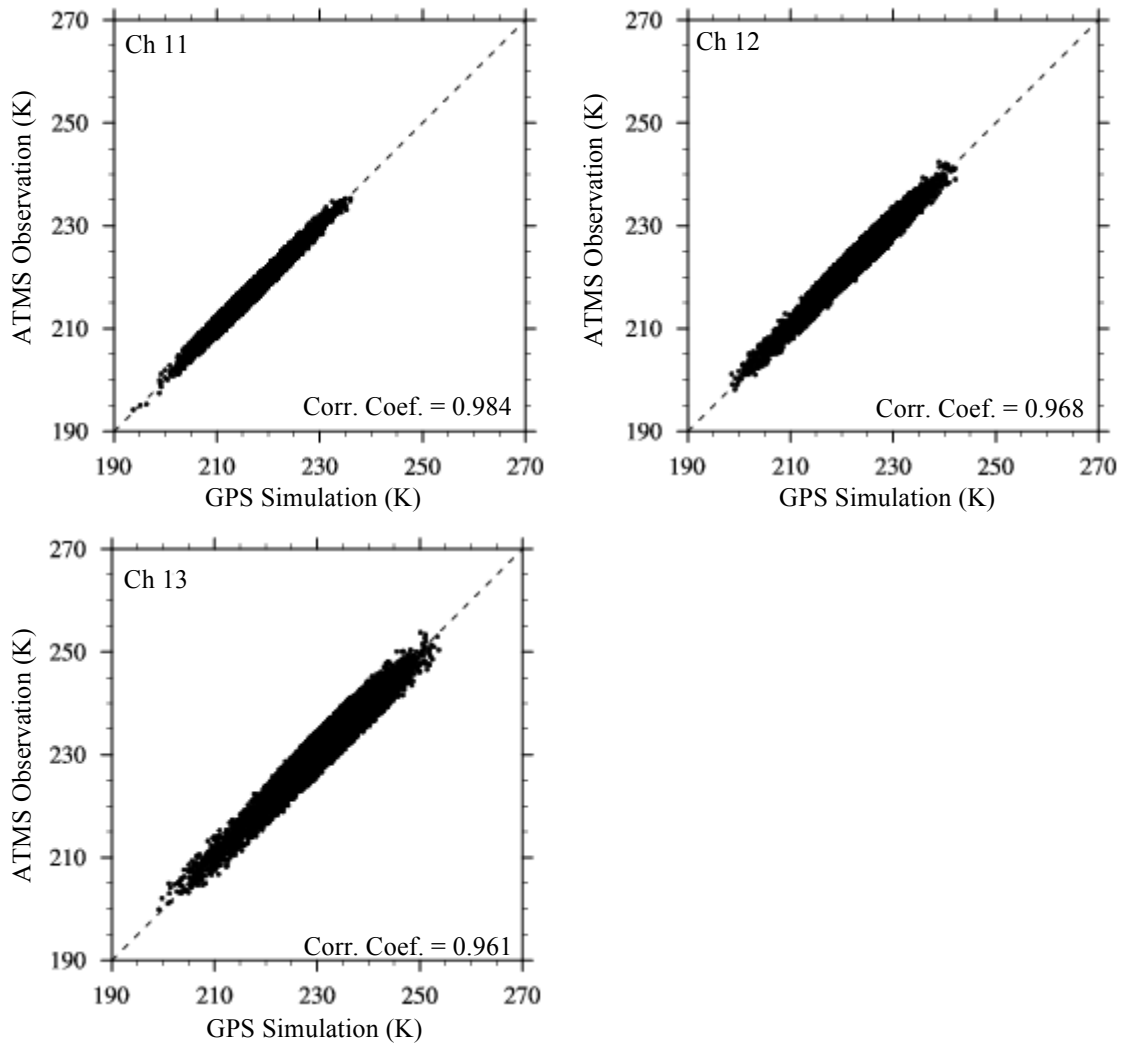


Fig. 4: Scatter plots of brightness temperature from ATMS observations and CRTM simulations with input from collocated COSMIC data under clear-sky over ocean between 60S-60N from December 10, 2011 to June 30, 2012.

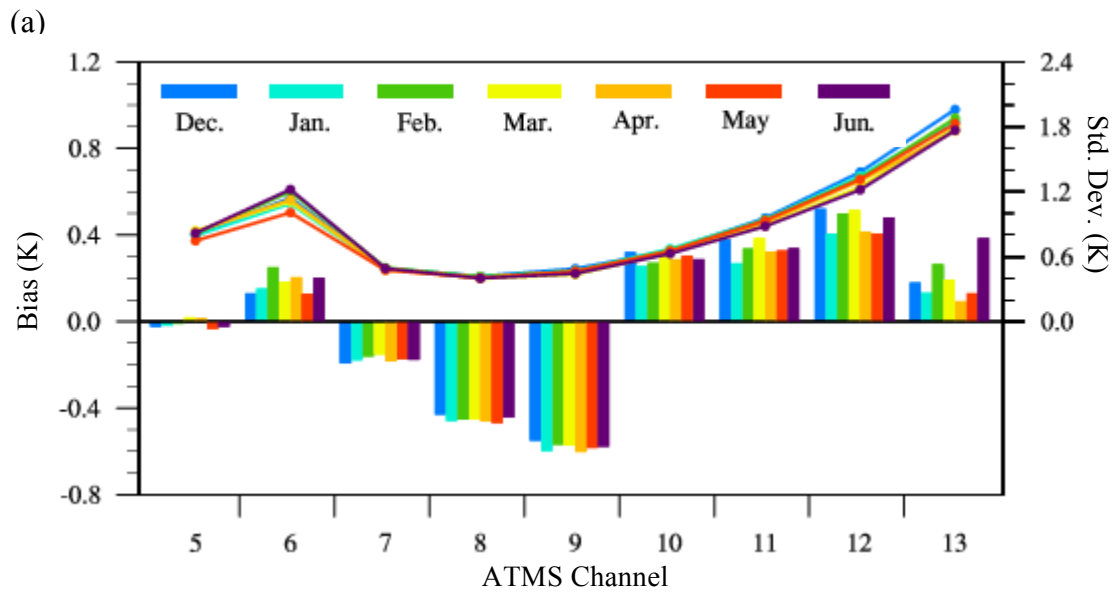


Fig. 5: Biases (bar) and standard deviations (curve) of the differences between ATMS observations and GPS RO simulations ( $O-B^{\text{GPS}}$ ) calculated for all collocated data under clear-sky conditions over ocean and between 60S-60N from December 10, 2011 to June 30, 2012.

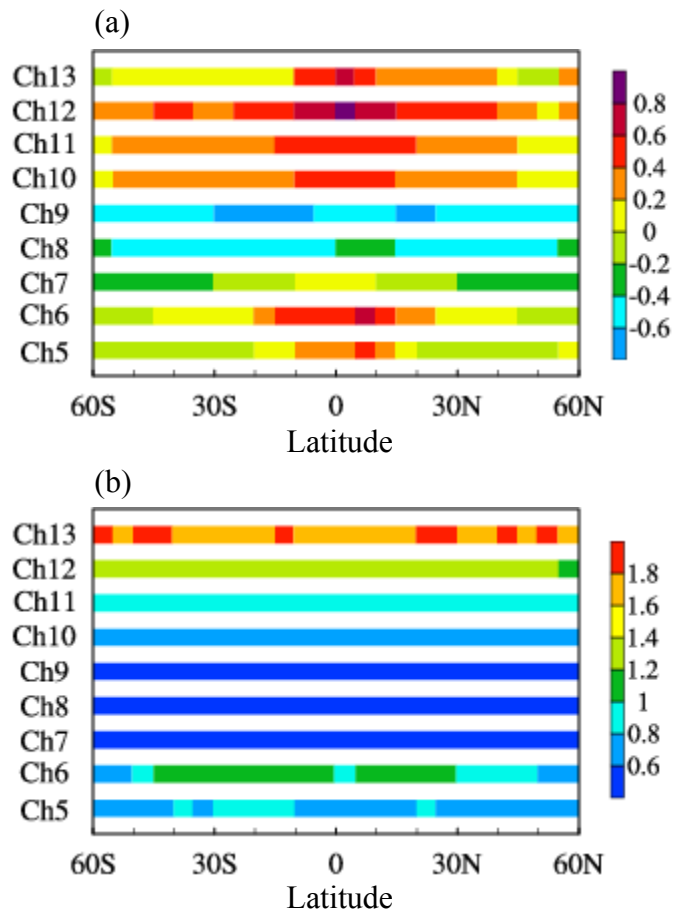
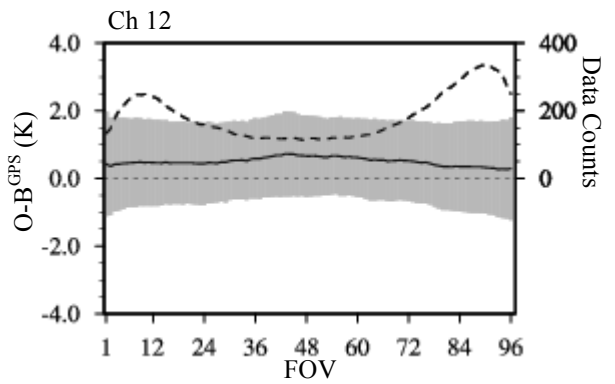
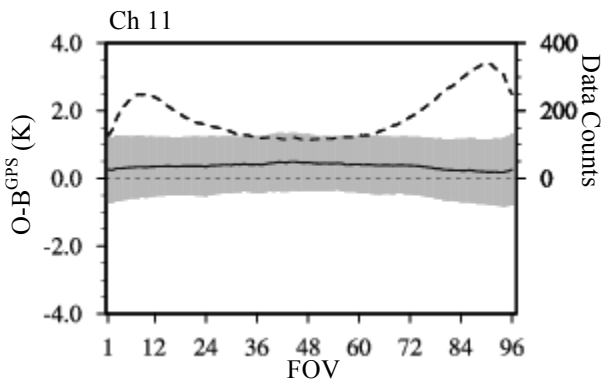
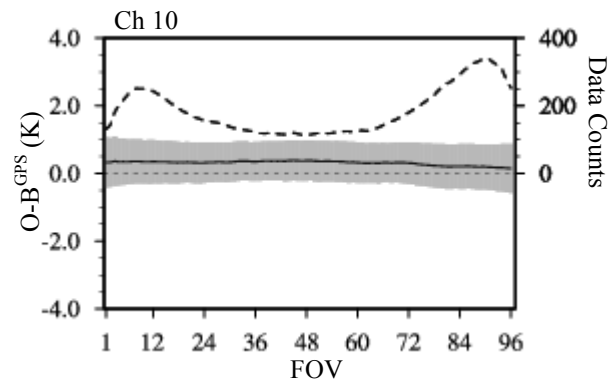
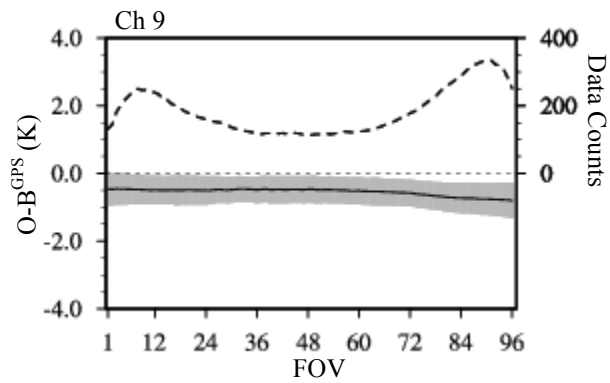
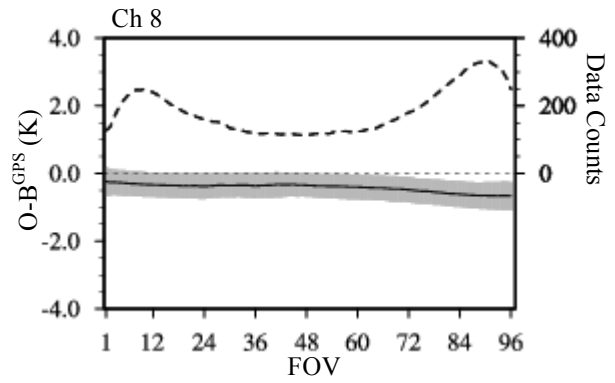
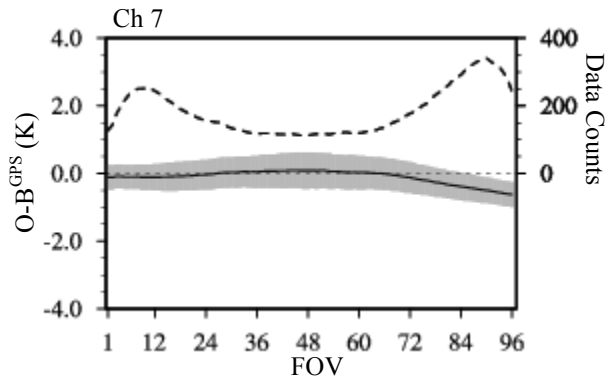
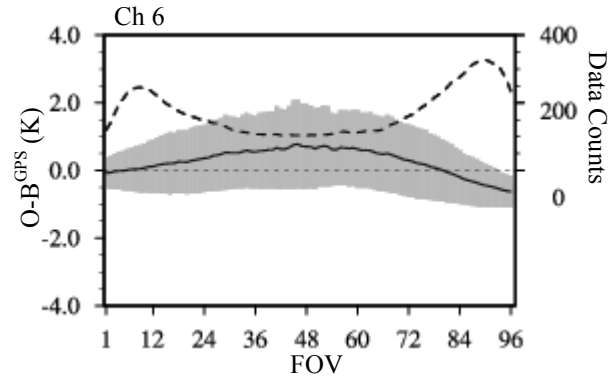
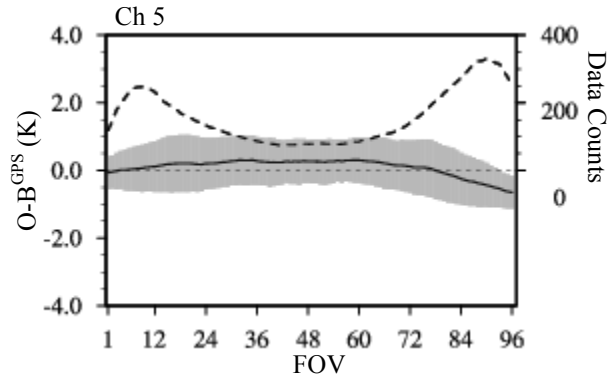


Fig. 6: Latitudinal distributions of (a) biases and (b) standard deviations calculated at  $5^\circ$  latitudinal interval for all collocated soundings under clear-sky conditions over ocean and between 60S-60N from December 10, 2011 to June 30, 2012.



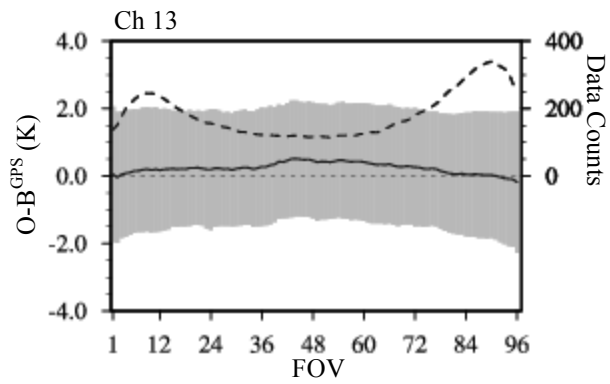


Fig. 7: Angular-dependence of brightness temperature biases (solid curve) and standard deviations (shaded area) estimated by the differences between ATMS observations and GPS RO simulations ( $O-B^{\text{GPS}}$ ) for collocated data under-clear sky over ocean between 60S-60N. The GPS RO profiles numbers collocated with ATMS data are also shown (dashed curve).

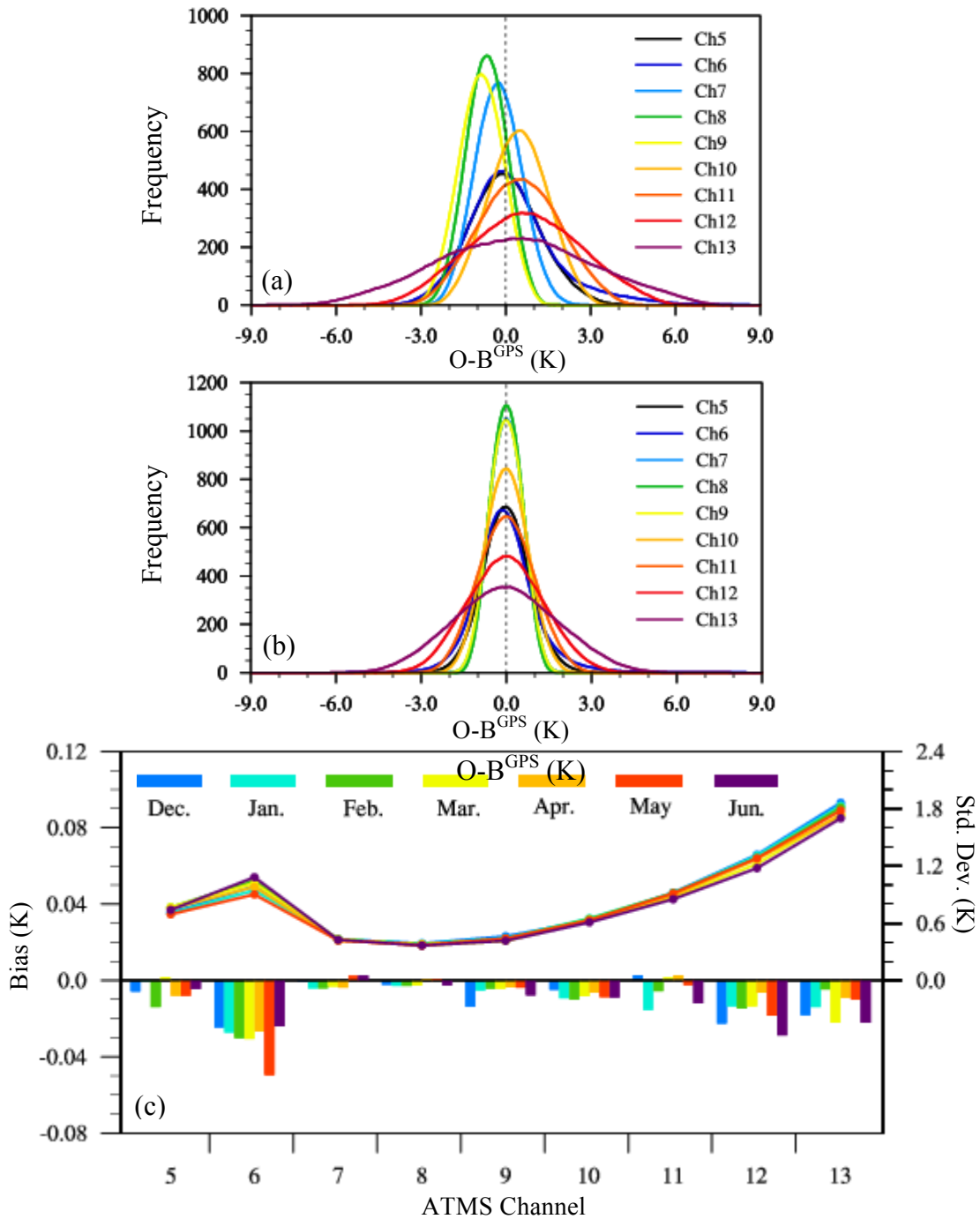


Fig. 8: Frequency distributions of O-B<sup>GPS</sup> differences for ATMS channels 5-13 before (a) and after (b) the GPS RO absolute post-launch calibration for all data from December 10, 2011 to June 30, 2012 under clear-sky conditions over ocean between 60S-60N. (c) Same as Fig. 5 except for the removal of the GPS RO derived scan bias.

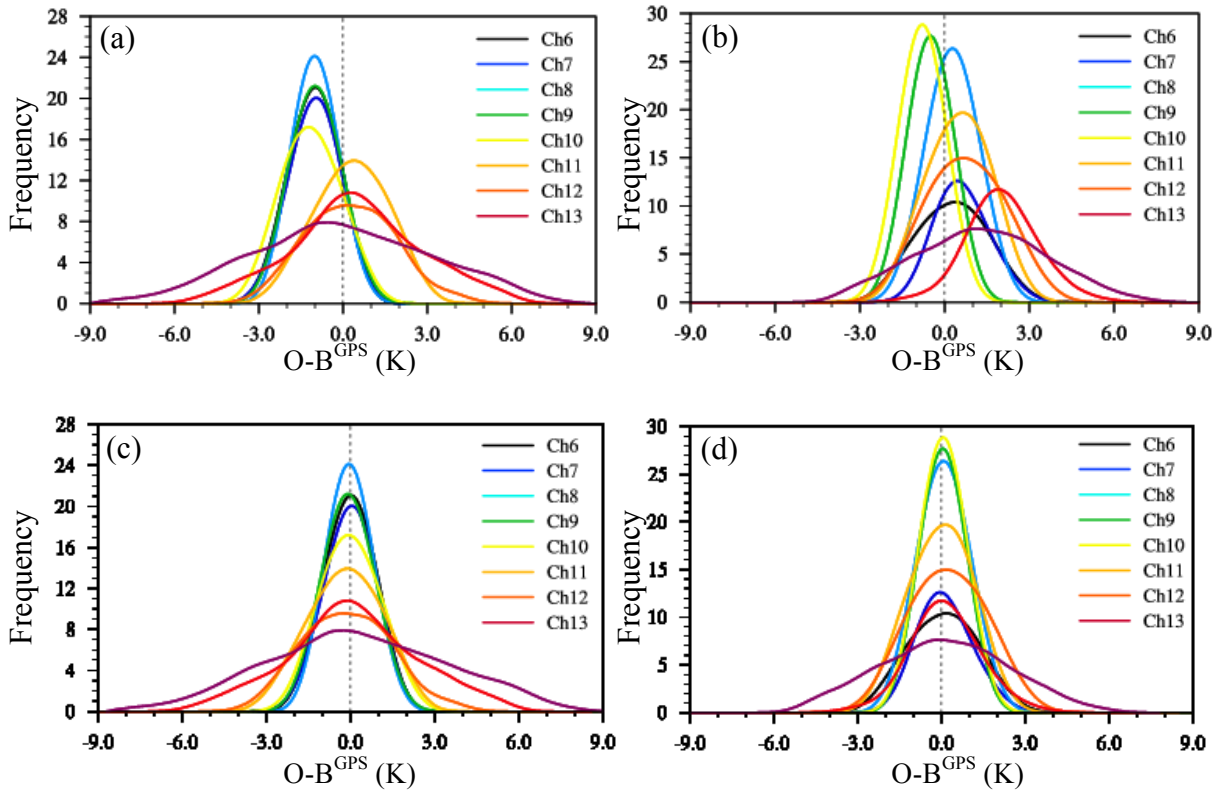
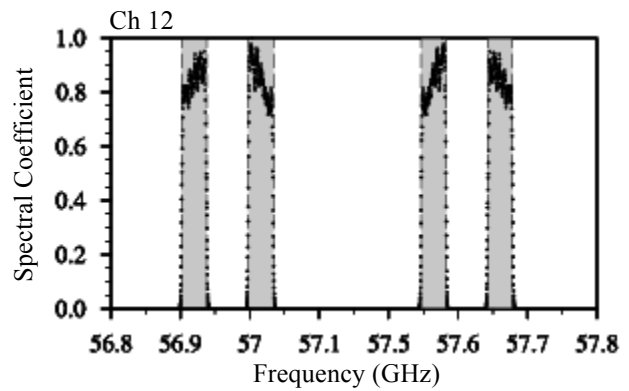
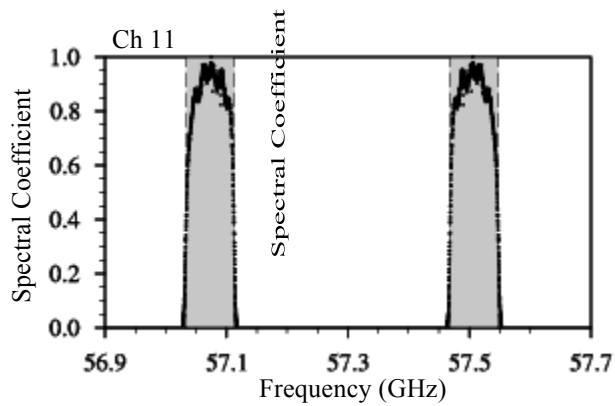
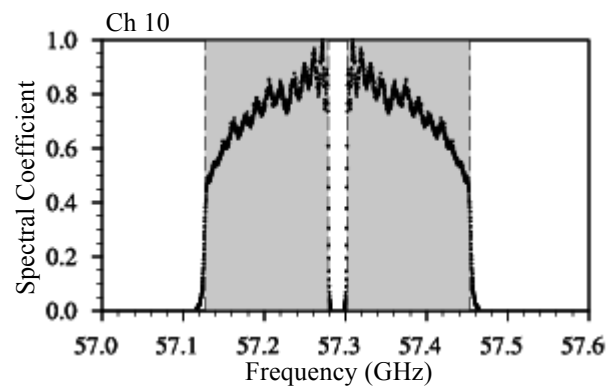
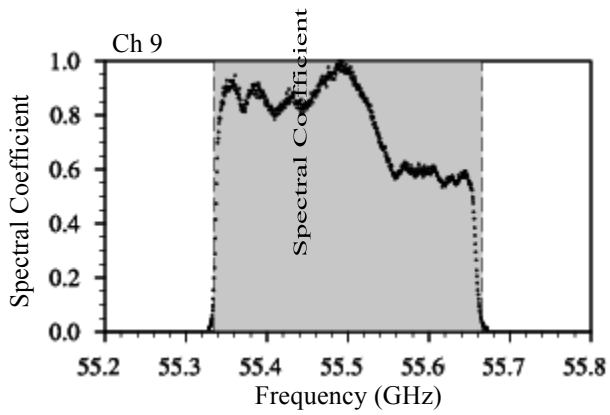
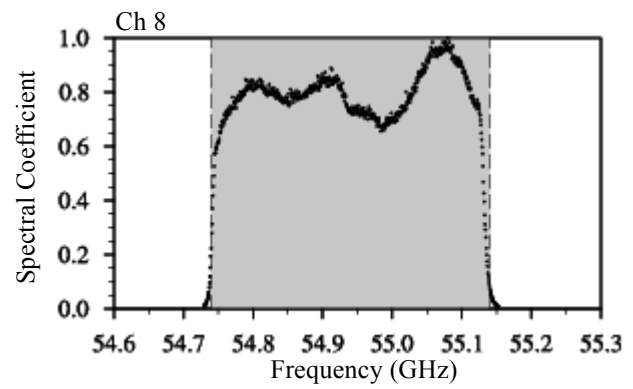
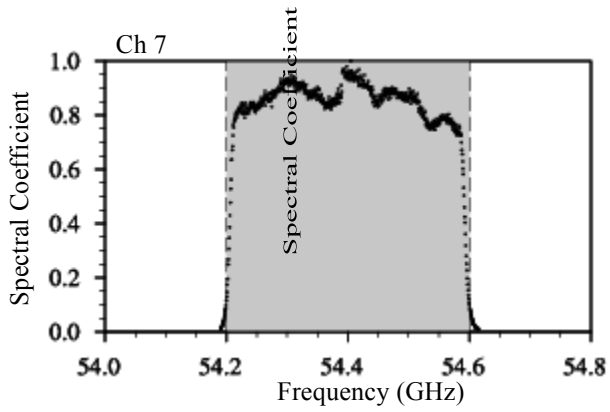
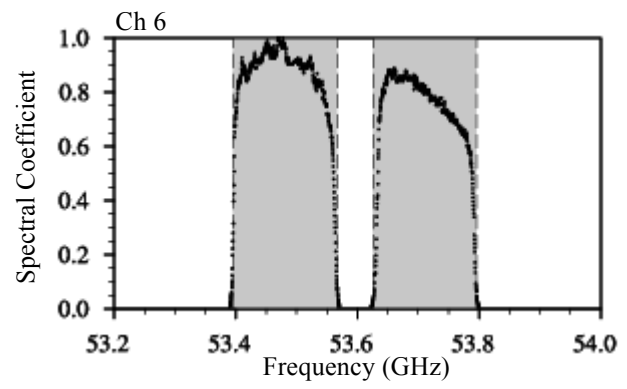
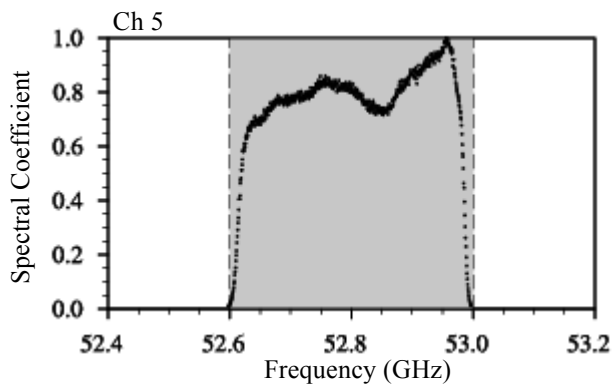


Fig. 9: Frequency distribution of  $O-B^{\text{GPS}}$  differences for ATMS channels 5-13 (a)-(b) before and (c)-(d) after the GPS RO absolute post-launch calibration for FOV1 (left panels) and nadir FOV 48 (right panels) using all data from December 10, 2011 to June 30, 2012 under clear-sky conditions over ocean between 60S-60N.



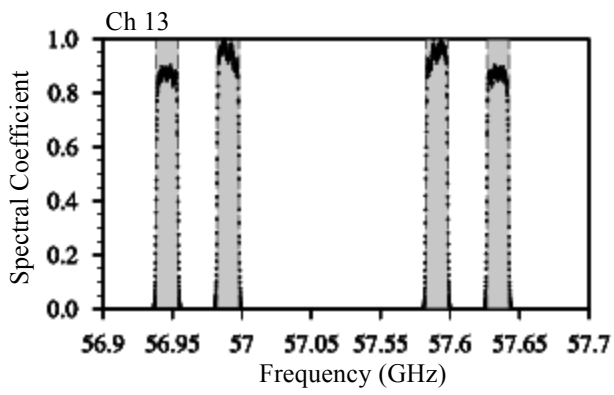


Fig. 10: Laboratory-measured SRF used in line-by-line model after -20dB truncation (black line) and the boxcar SRF using in CRTM (shading) for ATMS channels 5-13.

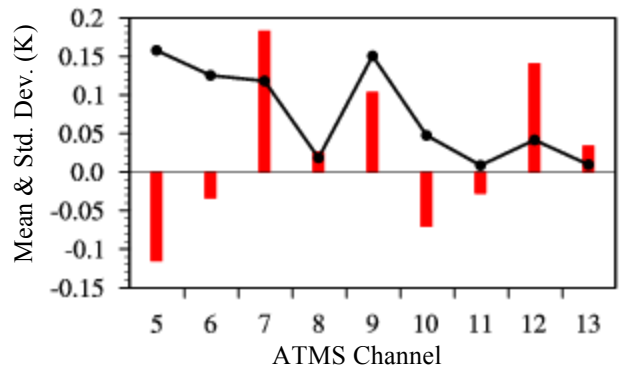


Fig. 11: Global means (bar) and standard deviations (curve) of the differences between GPS RO simulated brightness temperatures using the -20dB truncated SRF and the Boxcar SRF for one month data in January 2012 under clear-sky conditions over ocean within 60S-60N.